Corrugated Quantum Well Infrared Photodetector Focal Plane Array Test Results

August 1999

A. Goldberg and K. K. Choi
EO/IR Technology Branch, Army Research Laboratory, Adelphi, MD 20783
&
N.C. Das, A. La, and M. Jhabvala,
NASA Goddard Space Flight Center, Greenbelt, MD 20771
&
R.B. Bailey, and K.Vural
Rockwell Science Center, Thousand Oaks, CA 91360

ABSTRACT

The corrugated quantum-well infrared photodetector (C-QWIP) uses total internal reflection to couple normal incident light into the optically active quantum wells. The coupling efficiency has been shown to be relatively independent of the pixel size and wavelength thus making the C-QWIP a candidate for detectors over the entire infrared spectrum. The broadband coupling efficiency of the C-QWIP makes it an ideal candidate for multiwavelength detectors. We fabricated and tested C-QWIP focal plane arrays (FPAs) with cutoff wavelengths of 11.2 and 16.2 μm. Each FPA has 256 × 256 pixels that are bump-bonded to a direct injection readout circuit. Both FPAs provided Infrared imagery with good aesthetic attributes. For the 11.2-μm FPA, background-limited performance (BLIP) was observed at 60 K with *f*/3 optics. For the 16.2-μm FPA, BLIP was observed at 38 K. Besides the reduction of dark current in C-QWIP structures, the measured internal quantum efficiency (η) remains to be high. The values for responsivity and quantum efficiency obtained from the FPA results agree well with those measured for single devices.

1. INTRODUCTION

Over the past few years, quantum-well infrared photodetectors (QWIPs) have developed to the point that they can now be considered a serious alternative to the incumbent mercury-cadmium telluride (MCT) technology for infrared detection. This is especially true in multicolor applications and for wavelengths beyond 12 μm (very long wavelength infrared or VLWIR), where MCT focal plane arrays (FPAs) become difficult to fabricate owing to the large relative changes in bandgap for small variations in material composition. In contrast, QWIP structures use the III-V material system for which the material growth and device processing technologies are more mature relative to those of II-VI materials like MCT.

For detection of infrared wavelengths beyond 12 μm, the energy gap becomes less than 0.1 eV. The fabrication of uniform, large-format arrays of MCT photodiodes for such applications has proven to be difficult. QWIPs hold great promise in this arena for two reasons. First, the material composition

Form SF298 Citation Data

Report Date *("DD MON YYYY")* 00081999	**Report Type** N/A	**Dates Covered (from... to)** *("DD MON YYYY")*

Title and Subtitle Corrugated Quantum Well Infrared Photodetector Focal Plane Array Test Results	**Contract or Grant Number**
	Program Element Number
Authors	**Project Number**
	Task Number
	Work Unit Number
Performing Organization Name(s) and Address(es) EO/IR Technology Branch Army Research Laboratory Adelphi, MD 20783	**Performing Organization Number(s)**
Sponsoring/Monitoring Agency Name(s) and Address(es)	**Monitoring Agency Acronym**
	Monitoring Agency Report Number(s)
Distribution/Availability Statement Approved for public release, distribution unlimited	
Supplementary Notes	
Abstract	
Subject Terms	
Document Classification unclassified	**Classification of SF298** unclassified
Classification of Abstract unclassified	**Limitation of Abstract** unlimited
Number of Pages 12	

(percentage of aluminum in the barrier layers) is not very challenging for the commonly used molecular beam epitaxy (MBE) technique. Second, the quantum-well widths needed for such detectors are generally greater than those used for QWIPs in the 8 to 12 μm region of the spectrum. This allows for less variation of the well widths (as a percentage of the mean) for long wavelength QWIPs relative to those designed for shorter wavelengths.

There are, however, several issues that have kept QWIPs from being generally accepted as a detector structure for VLWIR applications. These issues are basically the same ones that confront QWIPs operating in the more conventional 3 to 5 μm (mid-wave infrared or MWIR) and 8 to 12 μm (long wave infrared or LWIR) bands. The two most important of these issues are: (1) high dark current and (2) low responsivity of QWIPs relative to MCT detectors operating in the same wavelength range and at the same temperature.

The first issue, that of the relatively high dark current of QWIPs with respect to MCT, does not have the overriding importance for VLWIR applications as it does for LWIR systems. Typically, VLWIR systems are designed for space-based platforms (since very little VLWIR light penetrates the atmosphere). That being the case, users are often willing to cool FPAs to temperatures as low as 40 K at which point the noise due to the dark current of VLWIR QWIPs is expected to be lower than noise from other sources.

The problem of low quantum efficiency of QWIPs relative to MCT is very important. QWIPs do not respond well to normally incident light because of the electric dipole quantum mechanical selection rule. Intersubband electron transitions (from the quantum-well ground state to an excited state) are allowed only if some component of the photon's electric field is perpendicular to the barrier. To absorb normally-incident light (for which the electric field is *parallel* to the barrier) some kind of optical coupling structure that rotates the propagation vector of the light must be incorporated in the pixel. Several different optical coupling structures have been proposed and demonstrated such as one-dimensional (linear) diffraction gratings,[1] two-dimensional gratings,[2] and "random" gratings.[3]

In this paper we will present test results from QWIP FPAs made with a relatively new optical coupling scheme, the corrugated QWIP (or C-QWIP). Two FPAs were fabricated and hybridized to a read-out integrated circuit (ROIC) chip. The first of these arrays had a wavelength of maximum response of 10.7 μm with a long wavelength cutoff of 11.2 μm; the second of these arrays had its peak wavelength at 15.0 μm and a long wavelength cutoff of 16.2 μm.

2. Device Fabrication

Two wafers, designated sample A and sample B, were grown and processed for this work. The details of the growth and fabrication processes have been discussed elsewhere[4] and will only be summarized here. The device structures, the so-called bound-to-quasibound QWIPs, were grown by MBE on

---

[1] G. Hasnain, B. F. Levine, C. G. Bethea, R. A. Logan, J. Walker, and R. J. Malik, Appl. Phys. Lett., **54**, 2515, 1989.
[2] J. Y. Anderson, L. Lundqvist, and Z. F. Paska, Appl. Phys. Lett., **59**, 857, 1991.
[3] G. Sarusi, B. F. Levine, S. J. Pearton, S. V. Bandera, and R. E. Liebenguth, Appl. Phys. Lett., **64**, 960, 1994.
[4] N.C. Das, K.K. Choi, A. C. Goldberg, A. La, M. Jhabvala, R.B. Bailey, and K.Vural, Fabrication and evaluation of 11.2 and 16.2 μm cutoff C-QWIP arrays, *Proceedings of the SPIE, Infrared Technology and Applications XXV*, Vol. 3387, Orlando, FL, 1999.

semi-insulating GaAs substrates. The well widths and barrier heights were designed such that sample A would have maximum response at 10.7 μm and sample B would have maximum response at 15.0 μm. In the fabrication of a C-QWIP, wet chemical etching is used which leaves the surface with triangular corrugations (hence the name corrugated QWIP) as shown in Figure 1 (a). Figure 1 (b) shows a top view of many pixels in an FPA. There is an unetched region in the center of each pixel where ohmic contact metal and the indium bump are deposited. The size of the unetched island generally depends on the indium bump size.

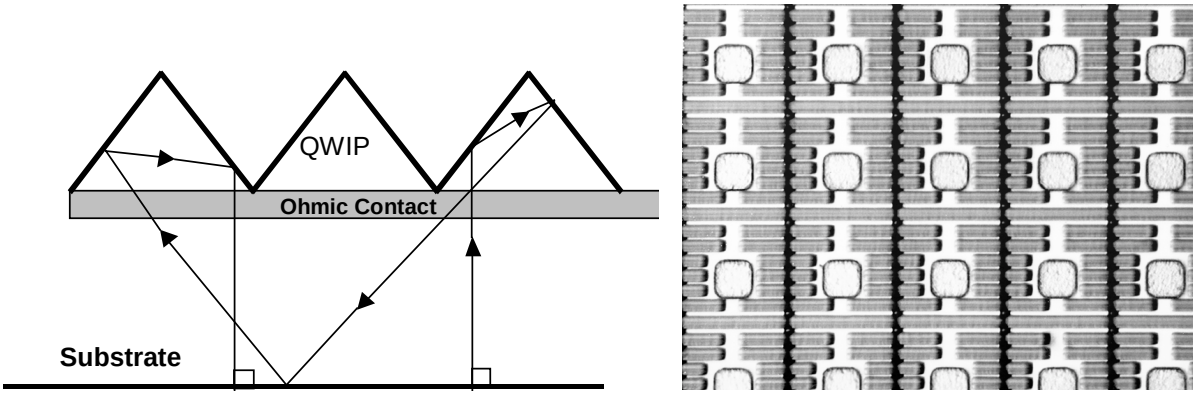

(a) (b)

Figure 1. The C-QWIP pixel in cross-section (a) showing a ray diagram of normally incident light as it suffers total internal reflection inside the pixel and a top view of several pixels in a focal plane array (b). The pixel size is 40×40 μm^2. There is an unetched island for the top contact metal and an unetched bridge to group several corrugations into one pixel.

The detectors were processed into arrays of 256 × 256 pixels and then were hybridized to Rockwell TCM2550 ROICs. Due to problems with wafer processing, the hybridization of sample A was done with no indium bumps on the detector side of the hybrid. As a result, large areas of the perimeter of the array, about 20 percent of the total number of pixels, were inoperable. The hybridization of sample B was much better, with only 1.6 percent of the pixels being inoperable.

A small piece of each wafer was used for single-pixel measurements. The results of these measurements are presented in detail elsewhere.[5] The wavelength of maximum response was 10.7 μm for sample A and 14.9 μm for sample B with long wavelength cutoffs of 11.2 μm and 16.2 μm, respectively. These results match the spectral responses predicted from the design recipe. The spectral response of typical devices from each wafer are shown in Figure 2.

The response spectra of the C-QWIP are compared with spectra from devices fabricated with no corrugation. Light was coupled to the noncorrugated devices through 45° wedges polished in the sides of their substrates. It is evident that the C-QWIP design preserves the entire response spectrum of the quantum well (as opposed to diffraction gratings, which tend to be highly resonant).

---

[5] K. K. Choi, C. J. Chen, L. P. Rohkinson, D. C. Tsui, N. C. Das, M. Jhobvala, M. Jiang, and T. Tamir, "Corrugated Quantum Well Infrared Detector Arrays," *IRIS Proceedings of the Specialty Group on Detectors*, Lexington, MA, 1999.

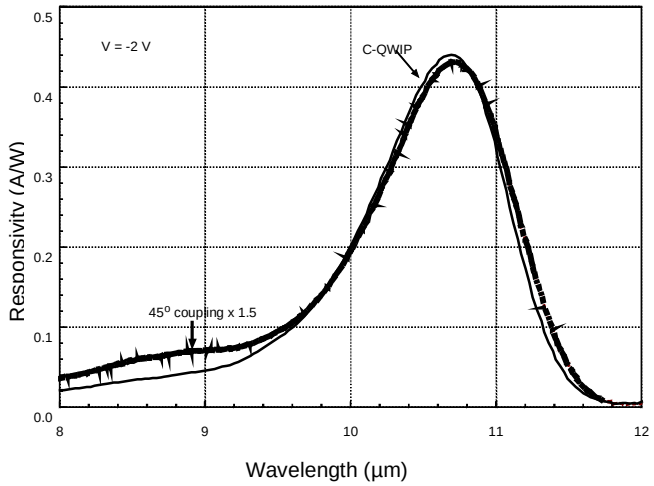

(a)

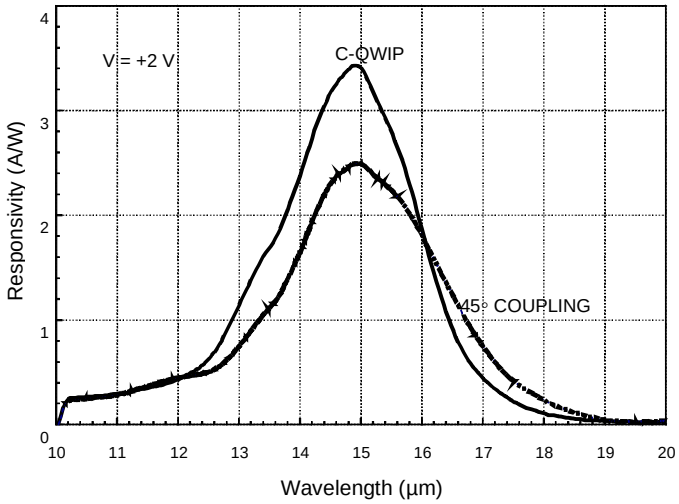

(b)

Figure 2. Spectral responsivity of samples A (a) and B (b). The wavelengths of maximum response are 10.7 μm and 14.9 μm, respectively.

3. FPA Test Results

3.1 Test Setup

Figure 3 is a block diagram of the system used to test the FPAs. The infrared source used was a CI-Systems Model SR-70 extended-area blackbody. Typically, the source temperature was varied from

20 °C to 40 °C. The system is capable of capturing many consecutive frames of images, either to the framegrabber's memory (at the frame rate of the camera) or directly to the hard disk (at a reduced rate).

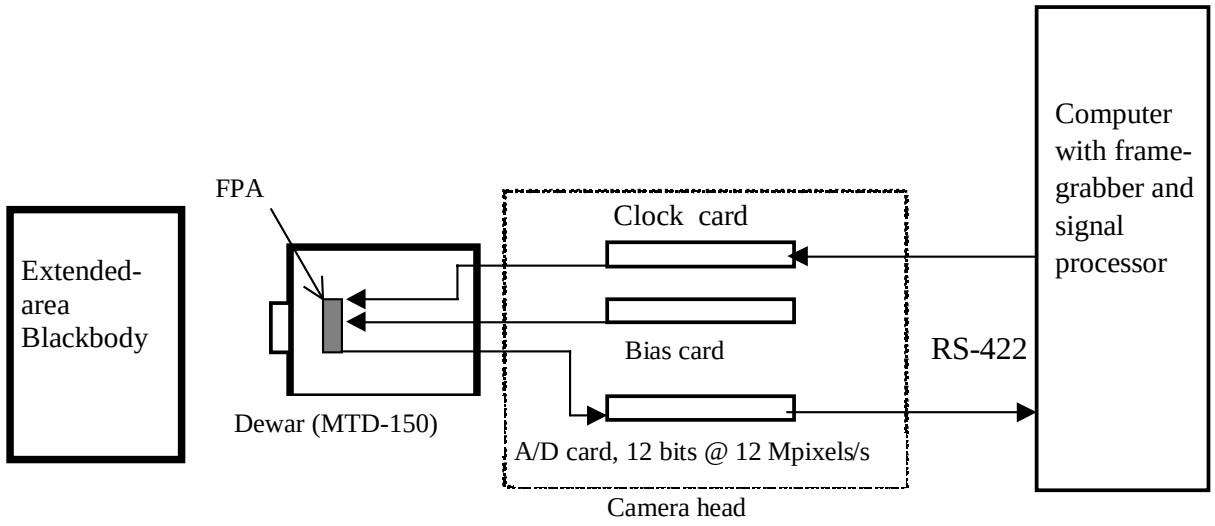

Figure 3. Block diagram of the FPA test setup. The clock card provides the six clock signals necessary to run the FPA and the bias card provides the 6 required DC bias levels. The signals from A/D card are transmitted to a computer over an RS-422 cable where they are converted to images by a framegrabber. The image data may then be stored to hard disk and/or displayed on a monitor.

The FPA drive electronics were built by SE-IR Corporation. The clock and bias generator cards are located in the "camera head" just outside the dewar. These cards provide the six clock signals (pixel clock, line clock, frame clock, etc.) and the dc bias levels (VDD, detector bias, etc.) necessary to run the FPA. The FPA output is fed into a 12-bit analog-to-digital (A/D) converter that is rated at 1.2×10^7 pixels/s with less than 1 count of noise in the least significant bit (LSB). The input-referred noise level is approximately 100 μV. The digitized signals from the A/D are transmitted to the computer over an RS-422 cable where they are converted to images by the framegrabber. The image data may then be stored to a hard disk and/or displayed on a monitor.

The tests on the arrays were done with the FPA installed in a liquid helium flow-through cryostat (Lakeshore MTD-150). The cryostat was equipped with an internal cooled aperture wheel that allowed for operation of the FPA under a wide range of background flux conditions (including zero-background for dark current measurements). The widest cold aperture corresponded to a field of view of *f*/3.

3.2 Results and Discussion

The bias conditions for the FPAs are shown in table 1. The bias function DSUB is the substrate bias. The actual bias across the detector is the difference between the value of DSUB and VDDA (the analog power bias). The conditions shown in Table 1 correspond to a bias across the detectors of –2 V (as measured from the indium bump contact on the detectors to the substrate). A small amount of bias may also be provided through the use of the DIGATE (direct injection gate) voltage. The other voltage levels on the ROIC do not significantly affect the bias on the detectors.

Table 1. Bias conditions used for the C-QWIP FPAs.

Bias name	Value (V)
VDDA	5.058
VDDD	4.998
DIGATE	3.135
COLPLUS	2.674
DEADPOT	2.502
DSUB	7.007

Generally, the FPA was run at a frame rate of 60 Hz. However, at low temperatures (~40 K) frame rates as low as 1 Hz were needed achieve integration times long enough to measure the dark current (under zero background conditions). For dark current measurements, the 0 field-of-view cold stop was placed in front of the FPA. The current was measured by integrating charge from the detectors for as long a time as necessary to fill the integration capacitor approximately half way to saturation. A number of frames (typically 50) were then collected and averaged. The current was then calculated using the expression

$$I = NG_{AD}\frac{C}{\tau} \quad \text{Amp} \tag{1}$$

where N is the number of counts, G_{AD} is the gain of the A/D converter (volts/count), C is the capacitance and τ is the integration time. The charge well capacity is 2×10^7 electrons when FPA is run in snapshot mode. The output voltage swing was 2.2 V. The well capacitance, therefore, was 1.45 pF. Similar data were collected with the shutter open (f/3 aperture) to measure the sum of the dark current and photocurrent.

3.2.1 Dark Current and BLIP Temperature

We show the results of dark current and photocurrent measurements on samples A and B in Figures 4 and 5, respectively. The dark current shows a clearly exponential dependence with temperature in both samples. The deviation from this behavior at the lowest temperatures may be due to the photon flux from the cold shield surfaces, which were at a temperature of approximately 80 K. If we define the temperature at which the current in the detectors generated by the background photon flux is equal to the dark current as the background-limited infrared performance (BLIP) temperature, then the BLIP temperature for sample A is approximately 60 K and that for sample B is 39 K. We can calculate the conversion efficiency (quantum efficiency × photoconductive gain) from the amount of photocurrent when the device is well below the BLIP temperature. For sample A, the background-induced current level is approximately 400 pA. This implies a peak conversion efficiency of 9 percent. Taking into account that the photoconductive gain measured on single-pixel devices from the same wafer was 0.25 at –2 V bias, the quantum efficiency is 20 percent. This value of quantum efficiency takes into account the 70 percent transmission of the dewar window but does not take into account the 30 percent loss of light from reflection off the substrate. The thermal activation energy calculated from the slope of the log of the dark current vs. $1/kT$ was 91 meV for sample A and 67 meV for sample B. These correspond to wavelengths of 13.6 μm and 18.5 μm, respectively. The background-induced photocurrent for sample B was 1.6×10^{-9} A and this implies a conversion efficiency of approximately 9 percent (similar to sample A). The gain measured on single pixels of sample B was approximately 1.0 at –2 V bias.[4] The quantum efficiency is therefore approximately 9 percent.

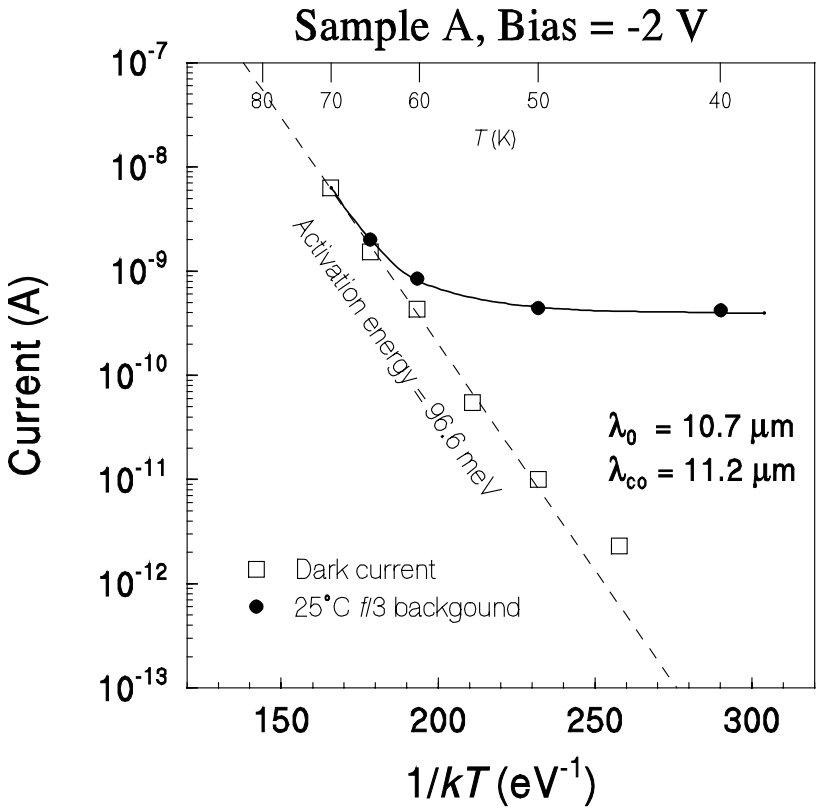

Figure 4. Mean dark current (squares) and total current (circles) for C-QWIP sample A as a function of temperature (described as 1/*kT*). The logarithmic behavior of the dark current with 1/*kT* defines a thermal activation energy of 96.6 meV.

Since the thermal activation energy depends strongly on the material growth parameters (well width, barrier height, etc.) its uniformity is a good indication of the quality of the epitaxial growth. Figure 6 shows a histogram (a) and an image (b) of the activation energy values for the pixels in sample A and Figure 7 shows the same information for sample B. We see that the standard deviation of the activation energy for the operable pixels of sample A (10.7 μm peak) was 1.5 meV, which was 1.55 percent of the mean. The standard deviation of the activation energy for sample B (15 μm peak) was 4.5 meV, which was 6.7 percent of the mean. This indicates that the QWIP structure parameters (well widths, AlGaAs composition, etc.) were very uniform in sample A but not nearly so in sample B.

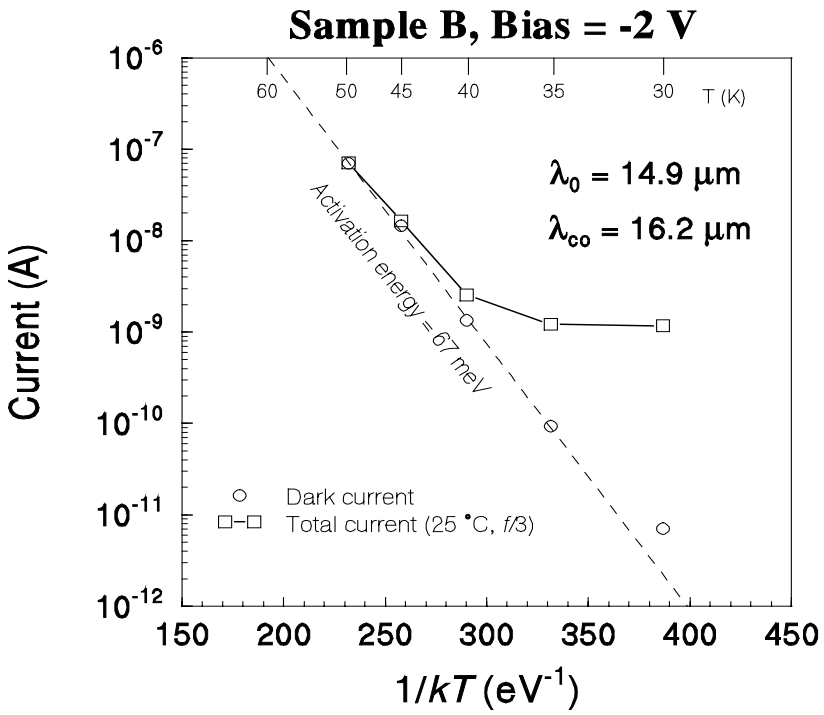

Figure 5. Mean dark current (squares) and total current (circles) for C-QWIP sample B as a function of temperature (described as 1/*kT*). The logarithmic behavior of the dark current with 1/*kT* defines a thermal activation energy of 67 meV.

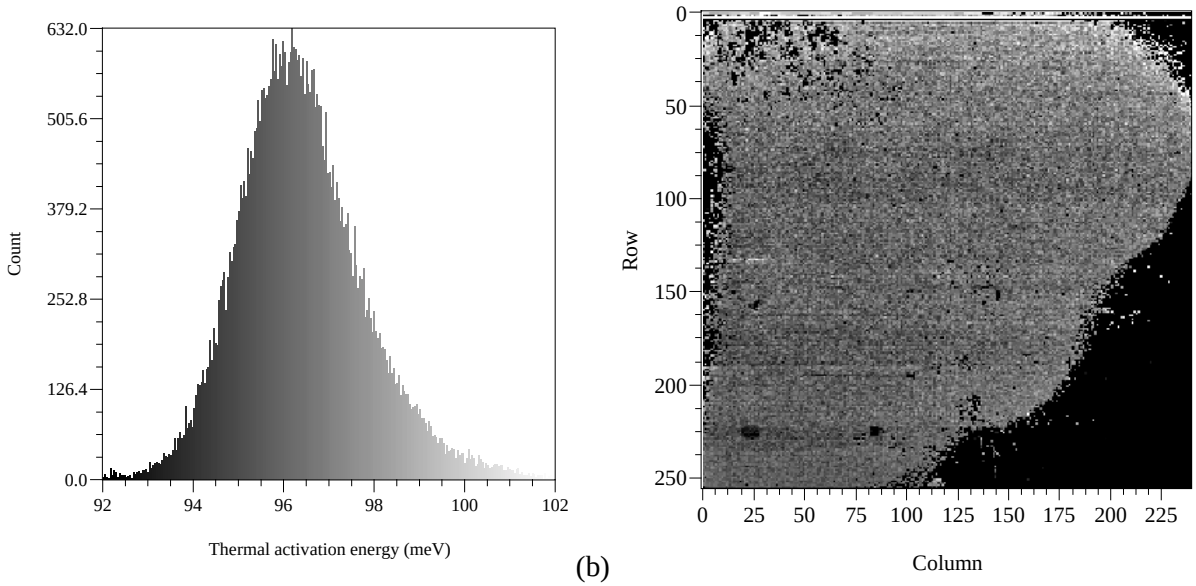

Figure 6. The histogram (a) and image (b) of the thermal activation energies for the pixels in sample A. The mean activation energy was 96.6±1.5 meV. The black areas in the image are the regions where the ROIC and the detector array failed to contact each other during hybridization.

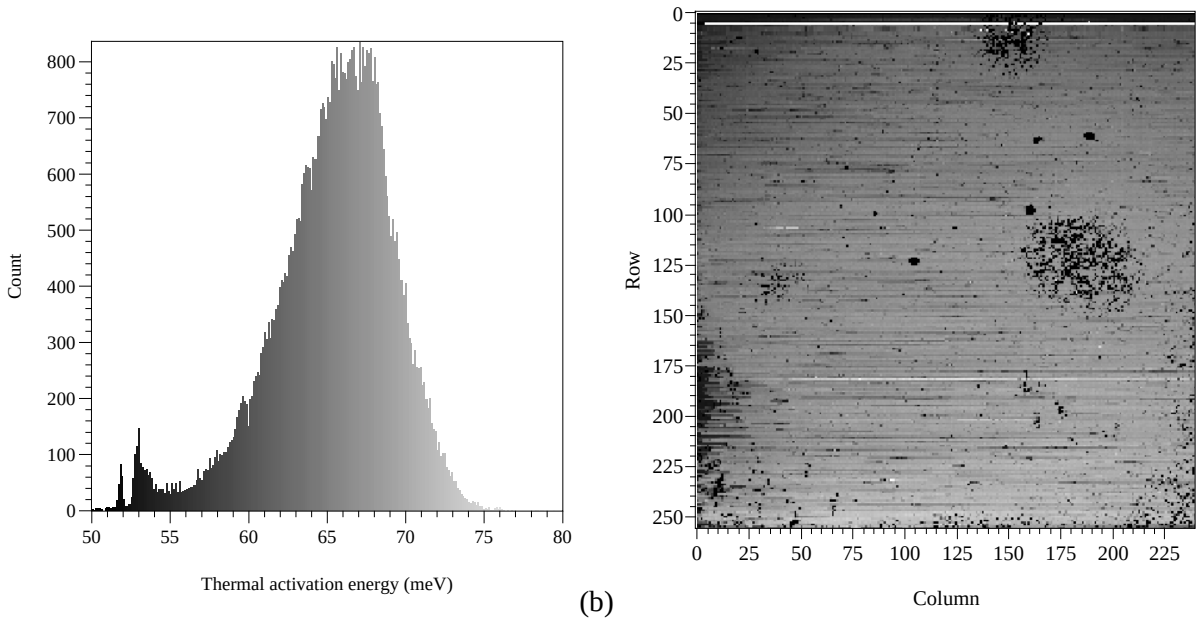

Figure 7. The histogram (a) and image (b) of the thermal activation energies for the pixels in sample B. The mean activation energy was 67±4.5 meV.

3.2.2 Noise-Equivalent Temperature Difference

Owing to an extraneous noise source inside the dewar, we were not able to accurately measure the noise-equivalent temperature difference on these arrays. This noise has also prevented us from performing accurate 3D-noise analysis on the FPAs as of this writing. However, we can estimate the value of the temporal NEΔT by making some reasonable assumptions. The noise of the A/D converter, Z_0, is known to be 0.6 -0.8 counts in the least significant bit when no signal is applied. The temporal noise at the input of the A/D will be proportional to the square root of the number of electrons that are collected in the charge well during each frame time. We assume that the number of electrons due to current from the detector is much greater than the number due to noise generated in the ROIC. The number of noise counts in each frame is then given by

$$Z_{total} = Z_0 + \sqrt{\frac{I\tau}{e}}\frac{e}{C}\frac{1}{G_{AD}} = Z_0 + \sqrt{\left(\frac{NG_{AD}C}{\tau}\right)\left(\frac{\tau}{e}\right)}\frac{e}{CG_{AD}} = Z_0 + \sqrt{\frac{Ne}{CG_{AD}}} \text{ Counts} \qquad (2)$$

where we have substituted the expression for the current in equation (1). If the number of signal counts is approximately 2000 (half of the total A/D range), the expected number of noise counts is approximately 2. The NEΔT can then be calculated by multiplying the noise by the measured temperature sensitivity. That is, the temperature difference represented by each A/D count. The temperature sensitivity was calculated from uncorrected image data taken at different scene temperatures. The estimated temporal NEΔT is then given by

$$NE\Delta T \approx Z_{total}\left(\frac{T_{HIGH} - T_{LOW}}{N_{HIGH} - N_{LOW}}\right) \text{ °C} \qquad (3)$$

where T_{HIGH} and T_{LOW} are the high and low scene temperatures, respectively and N_{HIGH} and N_{LOW} are the high and low response counts, respectively. Using equation (3), the NEΔT was calculated for samples A and B. The results of these calculations are shown in Figure 8 for sample A at an operating temperature of 50 K and Figure 9 for sample B at T = 30 K. At the respective temperatures, both FPAs were background-limited. The mean NEΔT for the operable pixels of sample A was 30±2 mK and that for the entire array of sample B was 30±1.5 mK. The standard deviations of the NEΔT values imply that the uncorrected response nonuniformity was 6.67 percent for sample A and 5.0 percent for sample B. In Figure 10, we show the variation of the NEΔT of both FPAs with operating temperature. Figure 11 shows the variation of the nonuniformity of response (the standard deviation of the NEΔT distribution divided by the mean value of NEΔT) for each array as functions of temperature. The uncorrected nonuniformity improves (decreases) as the temperature is lowered, even for temperatures well below the BLIP temperature.

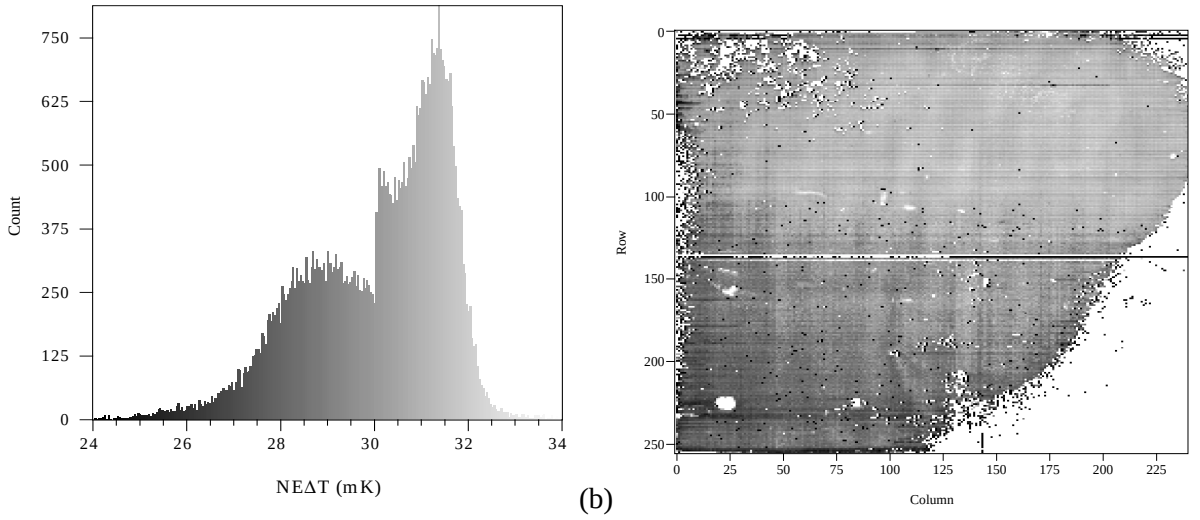

Figure 8. Estimated NEΔT histogram (a) and image (b) for sample A at a temperature of 50K. The mean NEΔT was 30±2 mK.

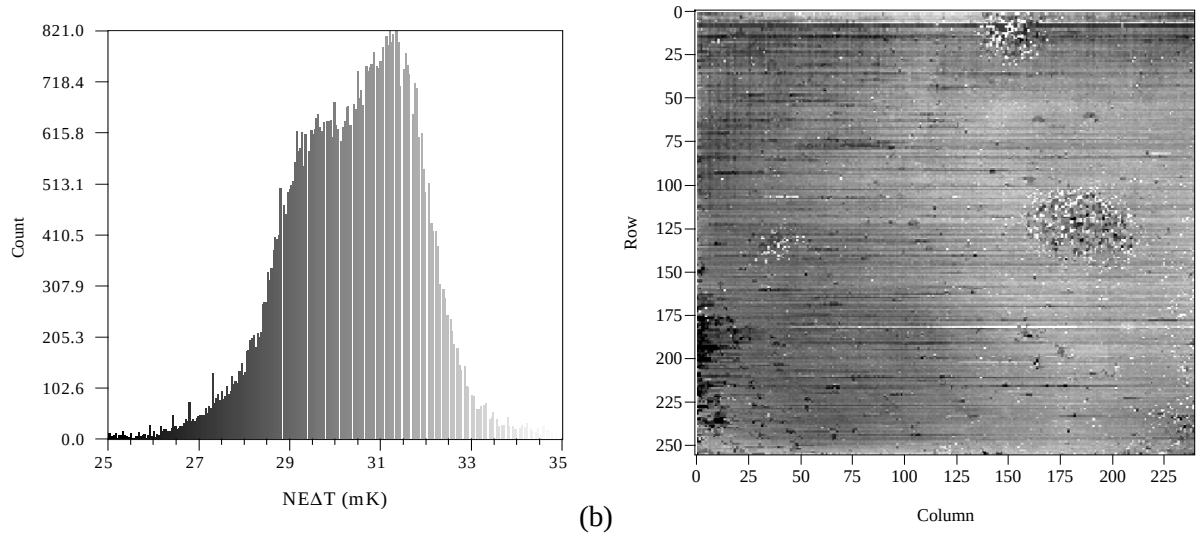

Figure 9. Estimated NEΔT histogram (a) and image (b) for sample B at a temperature of 30K. The mean NEΔT was 30±1.5 mK.

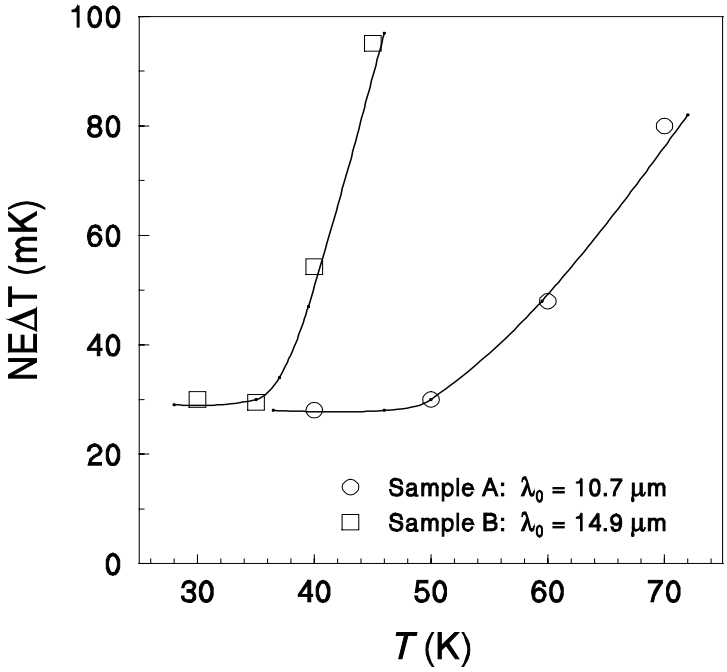

Figure 10. Variation of the NEΔT for sample A (circles) and sample B (squares) with temperature; the curves are simply guides to the eye.

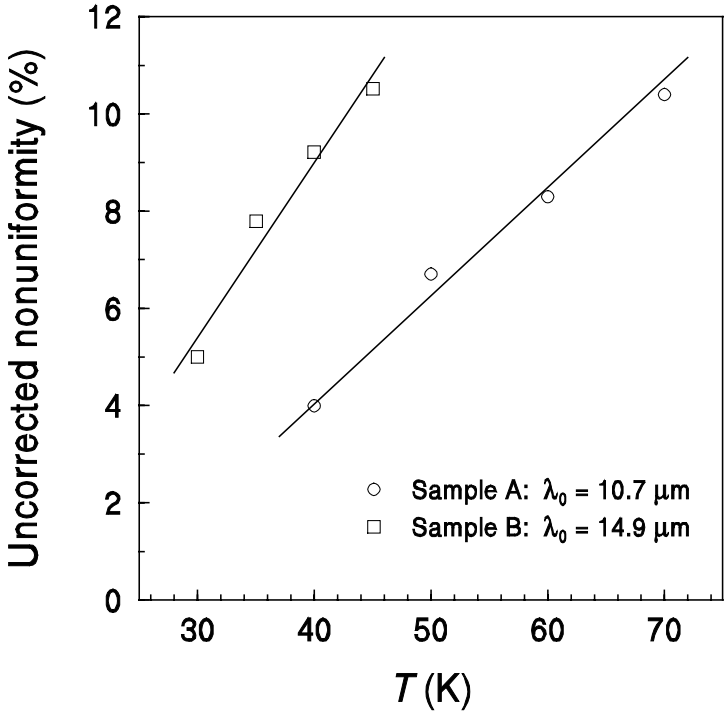

Figure 11. The uncorrected nonuniformity, the ratio of the standard deviation and the mean of the NEΔT for sample A (circles) and sample B (squares) as functions of temperature.

4. Summary and Conclusions

We have measured the imaging characteristics of two C-QWIP focal plane arrays. The FPAs exhibit relatively high values of quantum efficiency in agreement with previous single-pixel test results. The background-limited operating temperature (BLIP temperature) was found to be 60 K for the array with a peak wavelength of 10.7 μm and 39 K for the array with peak wavelength of 15 μm (for room-temperature background and an aperture of *f*/3) at a detector bias of –2 V. For an *f*/2 optical system, the BLIP temperatures for the arrays are expected to be slightly higher. Direct measurements of NEΔT could not be made due to extraneous system noise. However, under reasonable assumptions, NEΔT values for both FPAs were calculated to be approximately 30 mK at temperatures below the BLIP temperature. The uncorrected response nonuniformity at temperatures below the BLIP temperature was approximately 5 percent for both arrays. This shows that the wet chemical etch needed to form the corrugations is uniform enough to produce FPAs with good uniformity. The pixel operability of sample A (peak wavelength 10.7 μm) was only about 80 percent owing to the fact that it was hybridized with bumps only on the ROIC side of the hybrid. The operability of sample B (15 μm peak wavelength) was much better being 98.4 percent. In the coming year, we hope to fabricate and test FPAs with peak wavelength less than 9 μm. Given the high quantum efficiency seen in C-QWIP detectors, these FPAs are expected to have BLIP temperatures at or above 77 K. Finally, we show uncorrected laboratory images taken with the FPAs described in this paper in Figure 12.

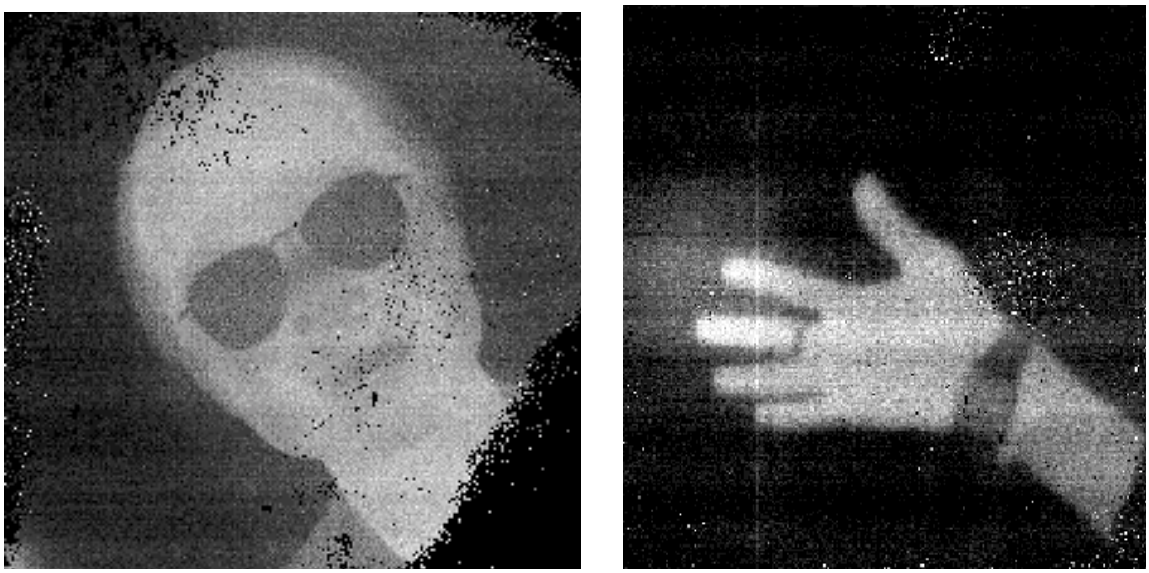

(a). (b).

Figure 12. Uncorrected IR imageries of a person taken with the 10.7 μm C-QWIP FPA at 64 K (a), and an image of a person's hand taken by the 15 μm C-QWIP FPA at 38 K (b).